Anisotropy of Magnetoresistance in HoB$_{12}$

A. Khoroshilov[a,b,*], V. Krasnorussky[b], A. Bogach[b], V. Glushkov[a,b], S. Demishev[a,b],
A. Levchenko[c], N. Shitsevalova[c], V. Filipov[c], S. Gabáni[d], K. Flachbart[d],
M. Anisimov[a], K. Siemensmeyer[e] and N. Sluchanko[a,b]

[a]Moscow Institute of Physics and Technology, Moscow Region, 141700 Russia
[b]Prokhorov General Physics Institute RAS, 119991 Moscow, Russia
[c]Institute for Problems of Materials Science, NASU, 03680 Kiev, Ukraine
[d]Institute of Experimental Physics, SAS, Watsonova 47, 040 01 Košice, Slovakia
[e]Hahn Meitner Institut Berlin, D 14109 Berlin, Germany

We present results of precision measurements of magnetoresistance of isotopically pure Ho^{11}B$_{12}$ at low temperatures $2 \div 10$ K in magnetic field up to 80 kOe of different orientation to the crystal axes. The data obtained revealed strong anisotropy of magnetoresistance and allowed us to reconstruct magnetic $H-T$ phase diagrams for main crystallographic directions $H \parallel$ [001], [110], and [111]. Analysis of magnetoresistance derivatives allowed to conclude in favor of two main magnetoresistance contributions. Among of them the negative quadratic component is attributed to charge carriers scattering on a magnetic clusters of Ho^{3+} ions ($4f$ component) and positive linear one may be explained in terms of scattering on a spin density waves ($5d$ component).

1. Introduction

Rare earth (RE) dodecaborides RB$_{12}$ crystallize in fcc crystal structure of UB$_{12}$ type (s.g. *Fm-3m*) where each RE ion is surrounded by 24 boron atoms forming the rigid cage of B_{24} truncated cubo-octahedron. Filling of the $4f$-shell in the set TbB$_{12}$–LuB$_{12}$ results in a wide variety of electronic and magnetic properties of dodecaborides. In current work we present magnetoresistance (MR) investigation of metallic antiferromagnet HoB$_{12}$ ($T_N \approx 7.4$ K [1–6]). According to specific heat, magnetization and transport measurements [2–6], HoB$_{12}$ exhibits rather complicated magnetic structure. Indeed the results of neutron diffraction experiments show that incommensurate amplitude-modulated antiferromagnetic (AF) structure is formed below T_N [4]. The topology of magnetic $H-T$ phase diagram of HoB$_{12}$ which was reconstructed in [3–5] exhibits both nearly isotropic behavior representing weak dependence of the direction of applied magnetic field for $T_N(H)$ and considerable anisotropic character for field induced magnetic transitions inside AF state. Therefore to shed more light on the mechanisms responsible for the ground state formation of HoB$_{12}$ we present here a detailed investigation of MR anisotropy.

2. Experimental details

The high quality single crystal of isotopically pure Ho^{11}B$_{12}$ ($T_N \approx 7.3$ K) was grown by vertical crucible-free inductive floating zone melting with multiple re-melting in an inert gas atmosphere on a setup described in details in [7]. The high quality of the crystal was controlled by X-ray diffraction, the Laue backscattering-patterns and electron microprobe analysis. Transverse magnetoresistance was studied in a temperature range 2–10 K in magnetic fields up to 80 kOe. In rotating experiment the direction of external magnetic field was varied in the range of angles $\varphi = 0-360°$ (where φ is an angle between vectors H and n, $n \parallel \langle 110 \rangle$ — the normal to the sample surface). Resistivity was measured by standard DC four-probe technique with the orientation of measuring current $I \parallel$ [110]. The high accuracy of temperature stabilization [$\Delta T \approx 0.001$ K at 4 K] was achieved with the help of commercial temperature controller TC 1.5/300 (Cryotel Ltd.) in combination with temperature sensors CERNOX-1050 (Lake Shore Cryotronics Inc.). The experimental setup was described in detail in [8].

3. Results and discussion

Figure 1 shows the magnetic field dependences of MR $\Delta\rho(H)/\rho = (\rho(H, T_0) - \rho(H = 0, T_0))/\rho(H = 0, T_0)$ at different temperatures below T_N for three main crystallographic directions $H \parallel$ [001], [110], and [111] (the parts (a), (b), (c) correspondingly). It is easy to see that MR changes dramatically with the temperature lowering and in AF state the amplitude of positive MR for H along [001] direction increases up to 80% ($T = 2.1$ K, Fig. 1a). On the contrary, essentially different MR behavior is observed for $H \parallel$ [111] with additional features attributed to field induced magnetic phase transitions in AF state (some of them are shown by separate symbols with arrows in Fig. 1). The strong anisotropy of magnetoresistance becomes much more evident in studies of the resistivity angular dependences $\rho(\varphi, H_0, T_0)$ (see, for example, Fig. 2). It is worth noting that all presented curves demonstrate sharp transitions ($\approx 5\%$ of MR changing) between angular domains with a moderate

———————
*corresponding author; e-mail: poligon-51@yandex.ru

(less than 0.2%) MR changes within the domain. These intervals of angles are translated over 180°, and one can distinguish three main domains: $[001] \pm 36°$, $[110] \pm 10°$ and $[111] - 18° \div [111] + 36°$. In the high fields $H \geq 55$ kOe the angular domain $[001] \pm 36°$ transforms to wide maximum at $[001]$ direction. It also should be noted that the magnetic scattering observed in MR has twofold symmetry axis.
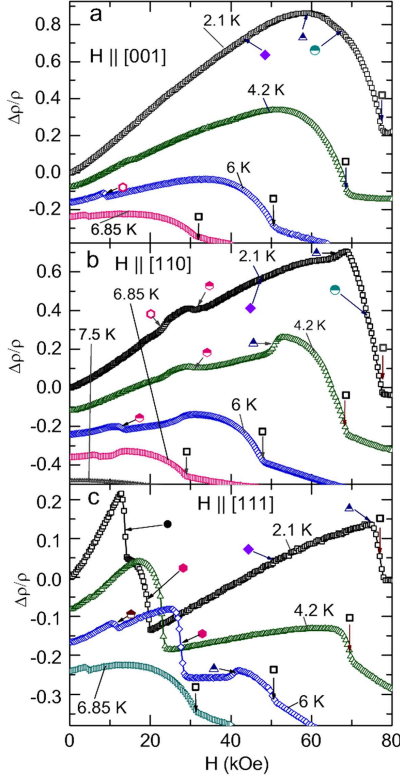

Fig. 1. Field dependences of MR for various temperatures at different orientations of the external field: (a) $\boldsymbol{H} \parallel [001]$, (b) $\boldsymbol{H} \parallel [110]$ and (c) $\boldsymbol{H} \parallel [111]$. The $\Delta\rho(H)/\rho$ curves are shifted down for convenience. Arrows mark the antiferromagnetic–paramagnetic (AF–P) and orientational magnetic phase transitions.

The high precision of the MR measurements allowed us to perform numerical differentiation of magnetic field dependences. Figure 3 demonstrates some examples of such derivation. The critical points on $\mathrm{d}(\Delta\rho/\rho(H))/\mathrm{d}H$ curves were attributed to orientational magnetic and AF–P phase transitions.

In order to separate contributions to MR we used approach developed in [9] which leads to the relation

$$\Delta\rho/\rho \approx -B(T)H^2 + A(T)H. \quad (1)$$

In Eq. (1) coefficient A of the linear term describes the amplitude of positive MR attributed to charge carriers scattering on the spin density waves (SDW) and B is characteristic of negative quadratic component attributed to scattering on the magnetic clusters of Ho^{3+} ions. Using formula

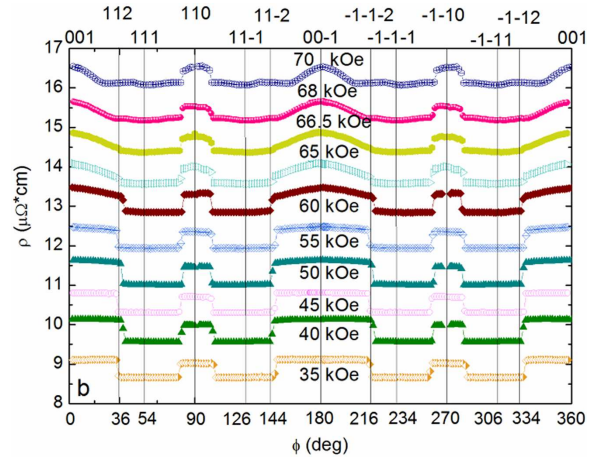$$\mathrm{d}(\Delta\rho(H)/\rho)/\mathrm{d}H \approx -2B(T)H + A(T) \quad (2)$$

Fig. 2. Angular dependences of resistivity $\rho(\varphi, H_0, T_0)$, at $T_0 = 2.1$ K for magnetic fields in the range 35–70 kOe. Indexes on the top show crystallographic directions corresponded to particular angles (curves are shifted on constant value for convenience).

for approximation of corresponded linear dependences of derivatives we have deduced B and A coefficients (Fig. 3). The analysis of the derivatives allowed us to reveal transition between the linear asymptotes connected with changes of the charge-carrier scattering on both magnetic clusters of Ho^{3+} ions and SDW. It was attributed as additional phase transition.

The data collection (see Figs. 1–3) was applied to reconstruct the $H-T$ magnetic phase diagram of Ho^{11}B$_{12}$ for main crystallographic directions (a) $\boldsymbol{H} \parallel [001]$, (b) $\boldsymbol{H} \parallel [110]$, (c) $\boldsymbol{H} \parallel [111]$. All symbols of the phase boundaries shown in Fig. 4 correspond to the symbols of magnetic phase transitions on the MR and derivative curves presented in Figs. 1 and 3, respectively. According to Fig. 4 the strong anisotropy is detected inside AF state of Ho^{11}B$_{12}$. To explain both the nature of intermediate phases and anisotropy of phase boundaries one should take into account the results of work [10] which describes the transition into the cage-glass state for RB$_{12}$ at liquid nitrogen temperatures (see also [1, 9]). Indeed, the transition to cage-glass state is accompanied by the appearance of disorder in the arrangement of Ho^{3+} ions inside B$_{24}$-truncated cubo-octahedrons resulting in the formation of magnetic nanosized clusters and consequently to the polarization of $5d$ conduction band states (the spin–polaron effect). Thus, the strong anisotropy and complex view of magnetic $H-T$ phase diagram of HoB$_{12}$ may be explained in terms of the formation of a combined magnetically ordered state of localized $4f$ moments of Ho^{3+} ions in combination with spin-polarized local areas of the $5d$ states-ferrons involved in the formation of spin density waves. The presence of the spin polarization was confirmed for HoB$_{12}$ in [3] where a ferromagnetic component of the order parameter was found in the magnetic neutron diffraction patterns. The detailed analysis of magnetic anisotropy of HoB$_{12}$ will be presented elsewhere.
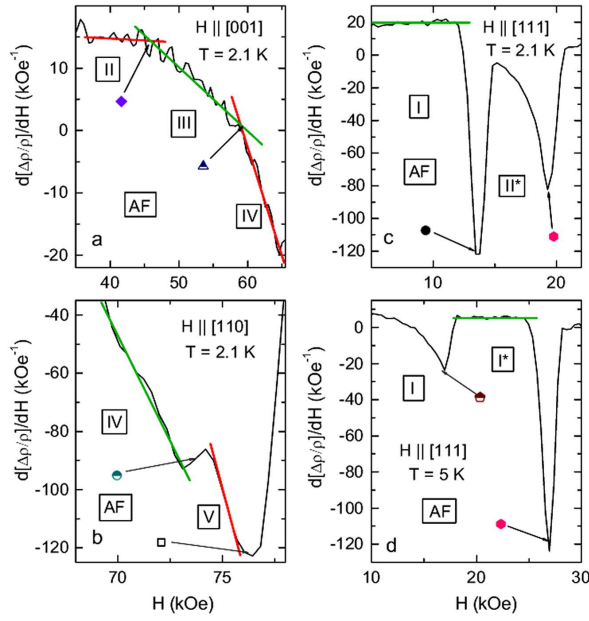
Fig. 3. Field dependences of MR derivatives $\mathrm{d}(\Delta\rho/\rho(H))/\mathrm{d}H$ for some temperatures and field directions. Colored lines show domains of linear approximation.
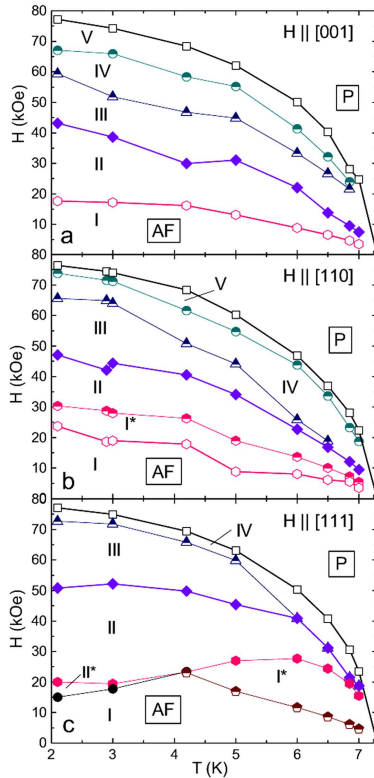

Fig. 4. Magnetic $H-T$ phase diagrams of $Ho^{11}B_{12}$ for three orientations of the external field: (a) $\boldsymbol{H} \parallel [001]$, (b) $\boldsymbol{H} \parallel [110]$ and (c) $\boldsymbol{H} \parallel [111]$. The solid lines are the guides for an eye.

4. Conclusions

We present the results of precise measurements of transverse MR of $Ho^{11}B_{12}$ in all range of angles φ in the plane perpendicular to [110] direction. It is reported that strong anisotropy of MR in $Ho^{11}B_{12}$ leads to different magnetic $H-T$ phase diagrams for three main crystallographic directions. Parameters of $4f$ and $5d$ scattering of charge carriers on localized magnetic moments and SDW were estimated. It is shown that two mechanisms of charge carriers scattering may be set to approximate the MR behavior in holmium dodecaboride.

References

[1] A. Menushenkov, A. Yaroslavtsev, I. Zaluzhnyy, A. Kuznetsov, R. Chernikov, N. Shitsevalova, V. Filipov, *JETP Lett.* **98**, 165 (2013).

[2] S. Gabáni, I. Bat'ko, K. Flachbart, T. Herrmannsdorfer, R. Konig, Y. Paderno, N. Shitsevalova, *J. Magn. Magn. Mater.* **207**, 131 (1999).

[3] K. Siemensmeyer, K. Habicht, Th. Lonkai, S. Mat'aš, S. Gabáni, N. Shitsevalova, E. Wulf, K. Flachbart, *J. Low Temp. Phys.* **146**, 516 (2007).

[4] A. Kohout, I. Batko, A. Czopnik, K. Flachbart, S. Mat'aš, M. Meissner, Y. Paderno, N. Shitsevalova, K. Siemensmeyer, *Phys. Rev. B* **70**, 224416 (2004).

[5] N. Sluchanko, A. Bogach, V. Glushkov, S. Demishev, N. Samarin, D. Sluchanko, A. Dukhnenko, A. Levchenko, *J. Exp. Theor. Phys.* **108**, 668 (2009).

[6] G. Pristáš, M. Reiffers, S. Gabáni, K. Flachbart, I. Radulev, K. Siemensmeyer, Yu. Paderno, N. Shitsevalova, *Czech. J. Phys.* **54**, D375 (2004).

[7] Yu. Paderno, V. Filipov, N. Shitsevalova, *AIP Conf. Proc.* **231**, 460 (1991).

[8] I. Lobanova, V. Glushkov, N. Sluchanko, S. Demishev, *Sci. Rep.* **6**, 22101 (2016).

[9] N. Sluchanko, A. Khoroshilov, M. Anisimov, A. Azarevich, A. Bogach, V. Glushkov, S. Demishev, V. Krasnorussky, V. Voronov, N. Shitsevalova, V. Filipov, A. Levchenko, G. Pristáš, S. Gabáni, K. Flachbart, *Phys. Rev. B* **91**, 235104 (2015).

[10] N. Sluchanko, A. Azarevich, A. Bogach, I. Vlasov, V. Glushkov, S. Demishev, A. Maksimov, I. Tartakovskii, E. Filatov, K. Flachbart, S. Gabani, V. Filipov, N. Shitsevalova, V. Moshchalkov, *J. Exp. Theor. Phys.* **113**, 468 (2011).